Astron. Astrophys. 326, 580–596 (1997)

ASTRONOMY
AND
ASTROPHYSICS

The radio galaxy 1138−262 at z=2.2: a giant elliptical galaxy at the center of a proto-cluster?

L. Pentericci[1], H.J.A. Röttgering[1], G.K. Miley[1], C.L. Carilli[2], and P. McCarthy[3]

[1] Leiden Observatory, P.O. Box 9513, 2300 RA Leiden, The Netherlands
[2] NRAO, PO Box 0, Socorro, NM, 87801
[3] The Observatories of the Carnegie Institution of Washington,813 Santa Barbara Street, Pasadena, California 91101

Received 7 March 1997 / Accepted 5 May 1997

Abstract. We present a detailed observational study of a remarkable radio galaxy at a redshift of z = 2.2: 1138-262.

This object was selected from our compendium of ultra steep spectrum radio sources on the basis of its distorted radio morphology. High resolution VLA radio observations show that the radio source consists of a series of knots and jet-like protrusions, with a sharp bend, strongly suggesting that the jet propagation is constrained by a dense external medium. Further evidence that 1138-262 resides in a dense environment comes from the extremely large rotation measure (6200 rad m^{-1}), the highest yet measured in a high redshift radio galaxy. This suggest that the source is at the center of an hot X-ray emitting halo, possibly a massive cooling flow ($\sim 500 M_{\odot}$yr^{-1}). Finally, a small emission line galaxy is observed 7″ to the north of the main galaxy: on the basis of both broad band and narrow band images we conclude that it is at the same redshift as 1138−262; therefore it is a further evidence of the overdense environment of the radio galaxy.

The bright K-band magnitude of 1138−262 suggest that the host of the radio source is a very massive galaxy, of the order $10^{12} M_{\odot}$. The K-band morphology can be fitted well by a classical De Vaucouleurs profile, indicating that 1138−262 is a well formed elliptical galaxy. However the UV/optical broad band morphology is very clumpy, consisting of a central region and a number of knots with sizes 10 to 15 kpc, which are systematically bluer that the central emission. All these components are embedded in a giant ($\sim$ 100 kpc) Lyα emission gas halo, which is also very clumpy and shows a high velocity dispersion. We argue that in the outer regions star formation is still occurring, either triggered by the passage of the radio jets or by the tidal interactions between the clumps that are falling on the parent galaxy.

Our favored interpretation of the observations is that 1138−262 is a massive elliptical galaxy, at the center of a dense, cluster-like region. The galaxy is still accreting mass from its environment, and will therefore become even more massive. This strongly supports the idea that 1138−262 will eventually become a cD galaxy.

Key words: galaxies: active – galaxies: radio – galaxies: clusters – galaxies: G 1138-262

1. Introduction

Until recently the only way to find significant numbers of galaxies with $z > 2$ was to observe the hosts of powerful radio sources (for a review see McCarthy1993). Although considerable progress has been recently made in finding radio-quiet galaxies at large redshifts (e.g Steidel 1996, Pascarelle et al. 1996), radio-loud galaxies are still an important probes of the early universe: the main aim of studying these object is to understand galaxy formation. At present more than 100 radio galaxies are known with $z > 2$ (Röttgering and Miley 1996). This redshift corresponds to a time when the universe was less than 20% of its present age and coincides with the epoch at which the space density of luminous quasars and radio galaxies was at a maximum (Dunlop and Peacock 1993).

Selecting ultra steep spectrum radio sources (USS) (radio spectral index $\alpha < -1$, where $S_{\nu} \propto \nu^{\alpha}$, with S_{ν} the flux density and ν the frequency) has proven to be one of the most efficient ways of finding distant galaxies (McCarthy 1993a). During the last few years some of us have carried out an ESO Key Programme, based on this method, to enlarge the sample of high redshift galaxies. Until now our USS radio sources survey has resulted in the discovery of more than 30 radio galaxies having $z > 2$ (Röttgering and Miley 1996). We are presently engaged in several follow up projects to study individual objects from the Key Program in more detail. We have previously presented extensive reports on three radio galaxies: 1243+036 at z=3.6, one of the most distant radio galaxies known, which shows a giant ($\sim$ 135 kpc) Lyα halo that is possibly rotating (van Ojik et al. 1996a); 0211−122 at z=2.3, which has an emission line spectrum with an anomalously low Lyα to NV ratio,

Send offprint requests to: L. Pentericci

probably due to a massive starburst (van Ojik et al. 1994); and 0943−242 at z=2.9, showing deep HI absorption against the extended Lyα emission (Röttgering et al. 1995). Here we report on another remarkable object discovered in the course of the ESO Key Programme, the radio galaxy 1138−262 at z= 2.2.

In Sect. 2 we describe why this object was selected for further study and discuss the observations and data analysis. In Sect. 3 the observational results are presented and physical parameters are deduced. Subsections describe the properties of the radio source (3.1), the morphology of the optical-IR continuum (3.2), the properties of the Lyα emission gas as deduced from narrow band imaging and high resolution spectroscopy (3.3). In Sect. 4, after a short summary of all the most important characteristics of the galaxy (4.1), we discuss the companion galaxy that is observed close to 1138−262 (4.2), the nature of the infrared continuum emission (4.3), the connection between Lyα emission and the radio parameters, with special regard to the bent radio structure (4.4); the interpretation of the radio polarization measurement (4.5); finally we discuss all our results in the context of different galaxy-formation and evolution scenarios, trying to assess the nature of 1138−262 (4.6). We summarize our conclusions in Sect. 5.

Throughout this paper we assume a Hubble constant of H_0 = 50 km s^{-1} Mpc^{-1} and a deceleration parameter of q_0 = 0.5

2. Selection and observations

The radio galaxy 1138−262 was selected from a compendium of USS radio sources being studied as a part of an ESO key programme (Röttgering et al. 1994); it is a radio source in the Parkes catalogue (Bolton et al. 1979) with a 408 MHz integrated flux density of 4.12 Jy and a very steep integrated radio spectrum with a spectral index of -1.3 between 80 MHz and 408 MHz. The radio source is also part of the Molonglo Reference Catalog/1 Jansky Radio Source Survey (McCarthy et al. 1996). Sources from the compendium were observed with the Very Large Array (VLA) at 1.5 GHz (Röttgering et al. 1994), as a preliminary for optical imaging and spectroscopy. From low resolution spectroscopy we found that 1138−262 has a redshift of 2.156 (van Ojik 1995). Further radio-polarimetric images, made as part of a high resolution survey of a large sample of powerful HZRGs (Carilli et al. 1997), revealed a peculiar clumpy morphology in the western radio lobe, and the highest known rotation measure of all studied HZRGs. Because of these extreme properties we selected PKS 1138−262 for follow up observations.

In this section we describe high resolution spectroscopy and imaging of the Lyα gas and optical-IR imaging in different color bands. A summary of the various observations, including data previously published that will be used in this analysis, is given in Table 1.

2.1. High resolution spectroscopy

High resolution spectroscopy of the Lyα emission line was carried out on the ESO New Technology Telescope (NTT), with the ESO Multi-Mode Instrument (EMMI) in the BLue Medium-Dispersion (BLMD) mode, on 30 April 1995. The detector was a Tektronix CCD having 1024^2 pixels with the scale along the slit of 0.37″ per pixels. The CCD was binned by a factor of two in the wavelength direction. Using a 2.5″ wide slit with ESO grating #3 we achieved a spectral resolution of 2.8 Å (full width at half maximum, FWHM). The total integration time of 7200s was split into three 45 minutes exposure, to facilitate removal of cosmic ray events. The slit orientation was approximately along the radio axis (PA=77°). Because the conditions were non photometric no spectroscopic standard was observed for flux calibration. The average seeing was $\simeq$ 1.3″. Reduction was carried out in the standard way using the IRAF reduction system of the US National Optical Astronomy Observatory. The raw spectra were bias subtracted and flat fielded; then the sky contribution was removed by subtracting a sky-spectrum obtained by fitting a polynomial to the intensities measured along the spatial direction, not including the spatial rows/columns where the target was positioned; finally wavelength calibration was performed by measuring the position on the CCD of known lines from a He-Ar calibration lamp, fitting a polynomial function to these data and applying the resultant calibration factors. The resulting accuracy of the calibration is better than 0.3Å.

2.2. Narrow band Ly α imaging

Narrow band imaging was carried out with the ESO NTT using EMMI in the Blue IMaGing (BIMG) mode. A narrow band filter (ESO filter #514) was used which has a central wavelength of 3840 Å and a bandpass width of 60 Å. The detector was a Tektronix CCD with 1024^2 pixels and a scale of 0.37″ per pixel. Two separate 1 hour exposures were taken, shifted by about 10″ with respect to each other to minimize problems due to flat-fielding and facilitate cosmic ray removal. The average seeing was 1.3″. Image reduction was carried out using the IRAF reduction package. The individual images were bias subtracted and flat fielded using twilight exposures. The images were then registered by shifting them in position by an amount determined from the location of several stars on the CCD near the object. After cosmic ray removal they were co-added. To improve the signal to noise, the resulting image was smoothed with a Gaussian function having a full width at half maximum of 1″ (3 pixels).

Astrometric calibration was carried out using the Guide Star Catalogue (GSC) image processing system of the Space Telescope Science Institute (Lasker et al. 1990), resulting in an accuracy of 0.7″.

2.3. Broad band imaging

An r-band image of a 2.2′ by 2.2′ region centered on the radio galaxy position was obtained with the ESO NTT using the Superb Seeing Imager (SUSI), on 29 April 1995. The detector was a Tektronix CCD with 1024^2 pixels and a scale of 0.12″ per pixel. A filter corresponding to Gunn r band (ESO filter #621) was used. Six exposures were made, each ten minutes long,

Table 1. Some Relevant Parameters of the Observations.

Date	Telescope	Frequency/Wavelength	Integration time/s	Resolution (FWHM)
26 Nov 1988	VLA A-array	1465 MHz	300	$1.5''$
18 Mar 1994	VLA A-array	4535,4885 MHz	600	$0.43''$
18 Mar 1994	VLA A-array	8085,8335 MHz	1200	$0.23''$
29 Apr 1995	ESO NTT + SUSI	Gunn r band	3600	$0.8''$
30 Apr 1995	ESO NTT + EMMI	3840/60 Å[a]	7200	$1.3''$
30 Apr 1995	ESO NTT + EMMI	B band	900	$1.3''$
30 Apr 1995	ESO NTT + EMMI	3600 to 4200 Å	8100	$1.3''\times$ 2.8 Å
14 Feb 1996	las Campanas du Pont	K_s band	6125	$0.6''$

[a] A narrow band filter centered at 3840Å and with bandpass width of 60Å was used.

shifted by about $10''$ with respect to each other. The seeing was $0.8''$ and the night was photometric. The images were bias-subtracted and flat fielded using IRAF. The flat field was derived from the median of the normalized image frames of similar exposures on different objects. The images were then registered by shifting them in position by an amount determined from the location of several stars on the CCD near the object. After cosmic ray removal they were co-added. Several stars which were visible on both the r-band image and the narrow band image were used to register the two images to an accuracy of $\simeq 0.1''$. Flux calibration was carried out with IRAF using standard stars in the field of Markarian A (Landolt 1992).

A B-band image of a $6.2'$ by $6.2'$ region centered on the object was obtained with the ESO NTT using EMMI in BIMG mode, on 30 April 1995. The seeing was $1.3''$ and the night was non-photometric. The detector was a Tektronix CCD with 1024^2 pixels and a scale of $0.37''$ per pixel. A filter corresponding to B-band (ESO filter #603) was used. Total integration time was 15 minutes. The image was bias subtracted and flat fielded using twilight exposures. Astrometric calibration was carried out in the same way as the r-band image.

1138-262 was observed in the K_s band at the 2.5-m du Pont Telescope at Las Campanas on February 14, 1996. The detector was a 256×256 HgCdTe based NICMOS3 array. The near IR camera (Persson et al. 1992) is located at the cassagrain focus and has a pixel scale of $0.348''$. Each K_s exposure was 35 seconds in duration and the telescope was offset after 5 exposures. A total of 175 exposures were obtained for a total integration time of 6125 seconds under photometric conditions with a seeing of $0.6''$ FWHM. Standard stars from Elias et al. (1982) were observed to establish the magnitude zero-points. Astrometric calibration was carried out in the same way as the r-band image.

3. Results

3.1. Radio polarimetric imaging

Fig. 1a shows the total intensity image at 8.1 GHz with $0.23''$ resolution, Fig. 1b shows the image at 4.5 GHz with a resolution of $0.43''$ and Figure.

The total extension of the radio emission is $15.8''$; in the adopted cosmology this is equivalent to 127 kpc.

A number of features have been labelled for reference in Fig. 1a, and in Table 2 we list for each of the source components the positions of the peaks, the peak surface brightness I, the integrated flux S (measured in a rectangular box around the components) at both frequencies and the spectral index α between 8.1 and 4.5 GHz computed from the integrated fluxes.

The eastern lobe (designated 'A') is a single component with a very steep spectral index. The western lobe (designated 'B') has a very complex structure: it consists of a series of knots all designated by subscripts, extending from component B1 towards west with a sharp bend in the south west direction at the location of component B3. We define the axis of the radio source as the line joining the peaks of components A, N and B1. This line forms an angle of -3° with respect to the the direction east-west. At the location of component B3 the western jet has a sharp bend towards south: and seems to split into two separate components, one including B4 which is extended, and the other including B5. This peculiar structure is also resembled by the distribution of the magnetic field vectors, and by the spectral index distribution, which shows that the southern region of the western jet has a flatter spectral index. The angle between the line joining the peaks of components B3 and B5 with the principal radio axis direction is $20^\circ \pm 2^\circ$.

At the location of component B5 there is a further bend towards south and the line joining components B5 and B6 forms a further $46^\circ \pm 2^\circ$ angle with the previous jet direction.

An image of the distribution of the spectral index between 8.1 and 4.5 GHz, obtained after convolving the two maps to the same resolution, is shown in Fig. 2, with contour levels superimposed. The spectral index distributions in the regions of steep gradients in the radio maps, are in general not true, but artifacts due to (i) the samplings in the uv space at the 2 frequencies that are not well matched and (ii) small residual differences in astrometry between the two maps. Most components of the radio source have very steep spectra, with indices < -1.5. The exceptions are component N and B1 which have a spectral index of -1.2. Notice that the spectral index distribution steepens with distance from the source center in component B.

Carilli et al. (1997) find that the lobes are substantially polarized: values of RM and depolarization between 8.2 and 4.5

Table 2. Results from the radio polarimetric imaging of 1138−262.

Comp.	$I_{8.1}$ mJy beam^{-1}	$I_{4.5}$ mJy beam^{-1}	$S_{8.1}$ mJy	$S_{4.5}$ mJy	RA J2000	Decl J2000	α
Int.			55.3	155.0			-1.8
A	7.39	31.79	15.0	48.3	$11^h40^m48.91^s$	$-26°29'9.2''$	-2.0
N	1.92	4.06	2.2	4.4	48.35^s	$8.7''$	-1.2
B1	5.47	12.45	7.0	14.1	48.29^s	$8.6''$	-1.2
B2	0.36	1.24	0.35	1.32	48.21^s	$8.9''$	-2.3
B3	5.87	18.17	13.7	32.2	48.15^s	$8.9''$	-1.5
B4	5.35	21.09	13.9	38.8	48.06^s	$9.8''$	-1.7
B5	0.74	4.93	2.27	9.7	47.98^s	$9.7''$	-2.5
B6	0.19	1.59	0.7	3.1	47.95^s	$10.6''$	-2.5

GHZ for the two components which showed fractional polarization $\geq$ 1.5% at both frequencies, are presented in Table 3. The extreme RM of component A and the large polarization asymmetry between the two lobes will be extensively discussed in Sect. 4.5.

An image of the projected magnetic field vectors of 1138−262, after correction for Faraday rotation, is presented in Fig. 3. The magnetic field is parallel to the jet in component A and B1; in component B4 the magnetic field is split into two component, one following the bending and the other parallel to the "tail" of hotspot B4.

We now discuss separately several issues concerning the radio morphology, and derive some important physical properties of the radio source.

3.1.1. Identification of the nucleus

Since none of the radio components has a flat spectrum, the location of the galaxy nucleus on the radio images is unclear: however several arguments lead us to identify it with component N, because (i) this component has a relatively flat spectral index (see Fig. 2) and (ii) it coincides spatially (the offset is $0.2'' \pm 0.7''$) with the brightest clump in the r-band image as well as the peak of the K_s-band image, while the only other radio component which shows an equally flat spectrum, B1, does not coincide with any optical components. Moreover (iii) the ratio of the flux density of component N to total source flux density is 3%, which is a typical value for core fraction of HZRGs (Carilli et al. 1997). Finally (iv) most powerful radio sources appear one sided, i.e. we observe only the jet on the side oriented towards the observer, which has a higher brightness due to the Doppler boosting (Bridle and Perley 1984). The spectral index of N is flatter than any other radio component in 1138, however it is steep compared to typical core components in powerful radio sources (e.g. Carilli et al. 1997, Lonsdale et al. 1993); HZRGs tend to have steeper spectral index than low redshift sources, but in our sample of 40 such sources, only 25% show cores with a spectral index steeper than -1. It is therefore possible that the nucleus has not yet been detected by our radio observations.

Table 3. Polarization parameters (From Carilli et al., 1997).

Comp.	$FP_{4.7}$ %	$FP_{8.2}$ %	$DP_{8.2}^{4.7}$	RM rad m^{-2}
A	4.4	6.8	0.65	6200
B4	2.9	8.7	0.33	630

3.1.2. Comparison with typical powerful radio sources

The radio structure of 1138−262 deviates from the morphology of typical ultra luminous radio galaxies in several important ways:
(i) Multiple hot spots are a common phenomenon in powerful radio sources (Laing 1988), but the clumpiness of 1138−262 is extreme. The knotty and distorted morphology of the B jet is comparable only to that of some compact steep spectrum radio sources (Fanti et al. 1990), which have scales 10 times smaller than that of 1138−262.
(ii) The spectral index distribution departs from the standard character of having the flattest spectral regions (besides the nucleus) associated with the radio hotspots, situated at the extremities of the lobes (Carilli et al. 1991). In 1138−262 there is a clear and systematic steepening of the spectral index along the jet B.
(iii) Typical powerful radio sources show a flat spectrum core while, as already discussed above, the flattest components of 1138−262 have $\alpha = -1.2$.
(iv) The magnetic field in each of the hotspots is oriented along the jet direction. This is opposite to the common characteristics of powerful radio sources of having the magnetic field oriented perpendicular to the jet direction at the edges of the hotspots (Muxlow and Garrington 1991). The series of knots in 1138−262 may actually be oblique shocks, for which fields parallel to the jet direction are not so rare. However $\overrightarrow{B}$ is parallel to the jet direction also in the terminal jet shocks (the outermost components) which is unusual.

3.1.3. Physical properties

Under the standard assumptions of equipartition (Miley 1980), and assuming that the plasma has unit filling factor, the synchrotron spectrum extends from 10^7 to 10^{11} Hz and that the

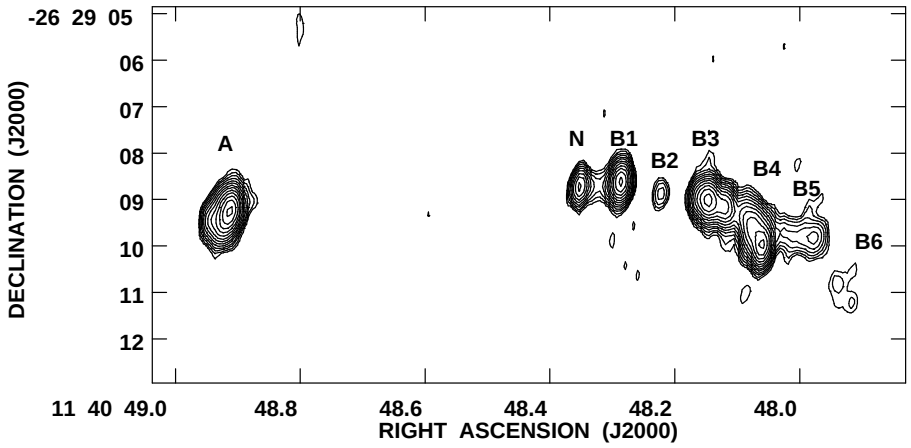

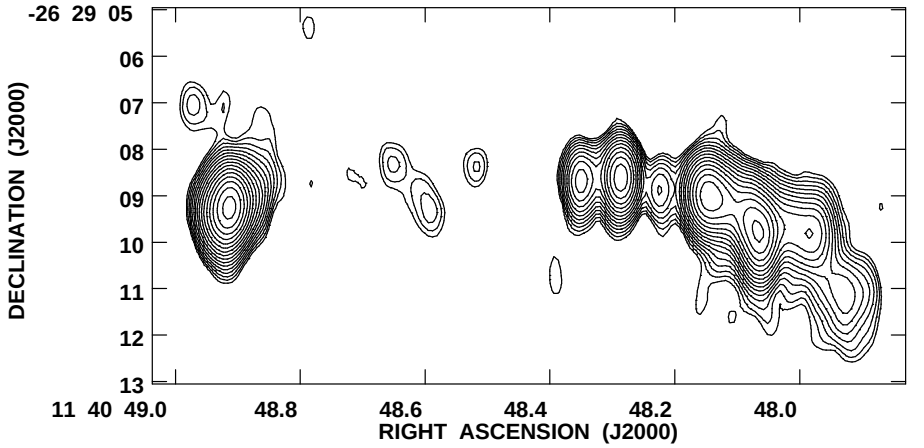

Fig. 1. a Contour representation of 1138−262 at 8.1 GHz with a Gaussian restoring beam of FWHM=0.25″. The contour levels are a geometric progression in steps of $2^{1/2}$, which implies a factor 2 change in surface brightness every two contours. The first contour level is at 0.11 mJy which is 3 times the off-source RMS noise on the image. **b** Contour representation of 1138−262 at 4.5 GHz with a Gaussian restoring beam of FWHM=0.44″ The contour levels are a geometric progression in steps of $2^{1/2}$. The first contour level is at 0.15 mJy which is 3 times the off-source RMS noise on the image.

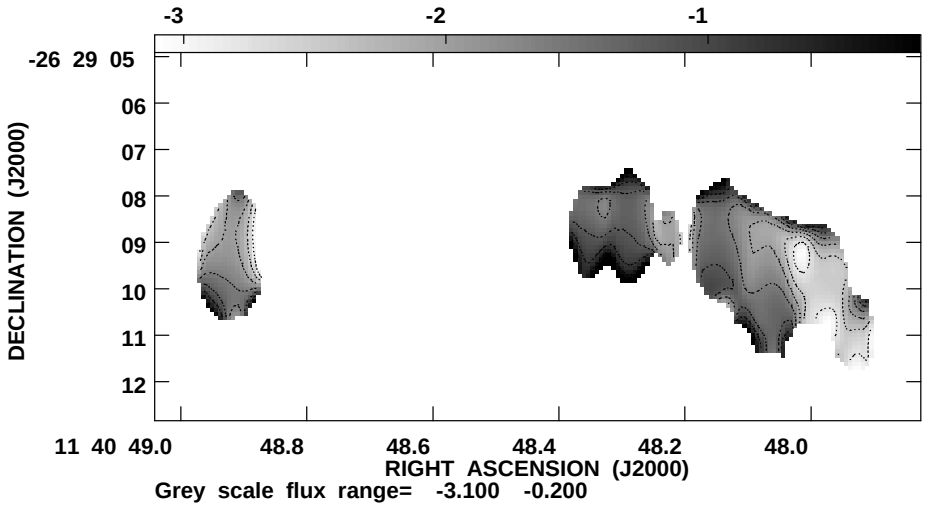

Fig. 2. A grey-scale representation of the two-point spectral index distribution between 8.1 GHz and 4.5 GHz of the radio emission from 1138−262, at a resolution of 0.43″. Only regions of the source where the signal to noise ratio is larger than 4 at both frequencies are shown. The contour levels are: -2.8,-2.4,-2.0,-1.6,-1.2,-0.8,-0.4,-0.2. The grey scale ranges from -3.1(white) to -0.2 (black).

ratio of energy in the heavy particles to that in electrons is one, we derived the minimum energy density u_{min} and the corresponding magnetic field strength B_{min}. In calculating the total minimum energies E_{min} we further assumed that the radio components are cylindrically symmetric. Finally in calculating the bolometric luminosities L_{TOT}, for those components which have a spectral index $\alpha < -1.3$, a two slope power law spectrum was assumed with a spectral index below 4.5 GHz (observed frame) of -1.3 equal to the integrated source spectral index between 80 and 408 MHz (Röttgering et al. 1995).

We can estimate the density of the external medium, assuming that the minimum pressure (of the relativistic particles) P_{min} are balanced either by ram pressure due to the propagation of the radio plasma at a velocity of a few thousands km s^{-1} (Carilli et al. 1991), or by static pressure exerted by a hot ($\simeq 10^7$ K) external medium, which is often found around powerful nearby radio galaxies (Crawford and Fabian 1989,

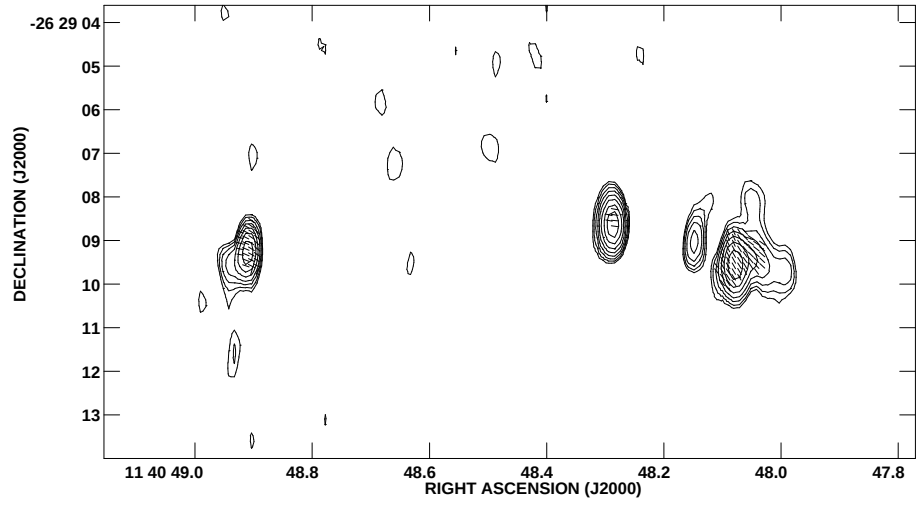

Fig. 3. An image of linear polarized intensity from 1138−262 at 8.2 GHz with a resolution of $0.43''$. The contour levels are a geometric progression in $2^{1/2}$. The first contour level is 0.075 mJy. The line segments show the orientation of the projected magnetic field vectors derived from the polarized emission.

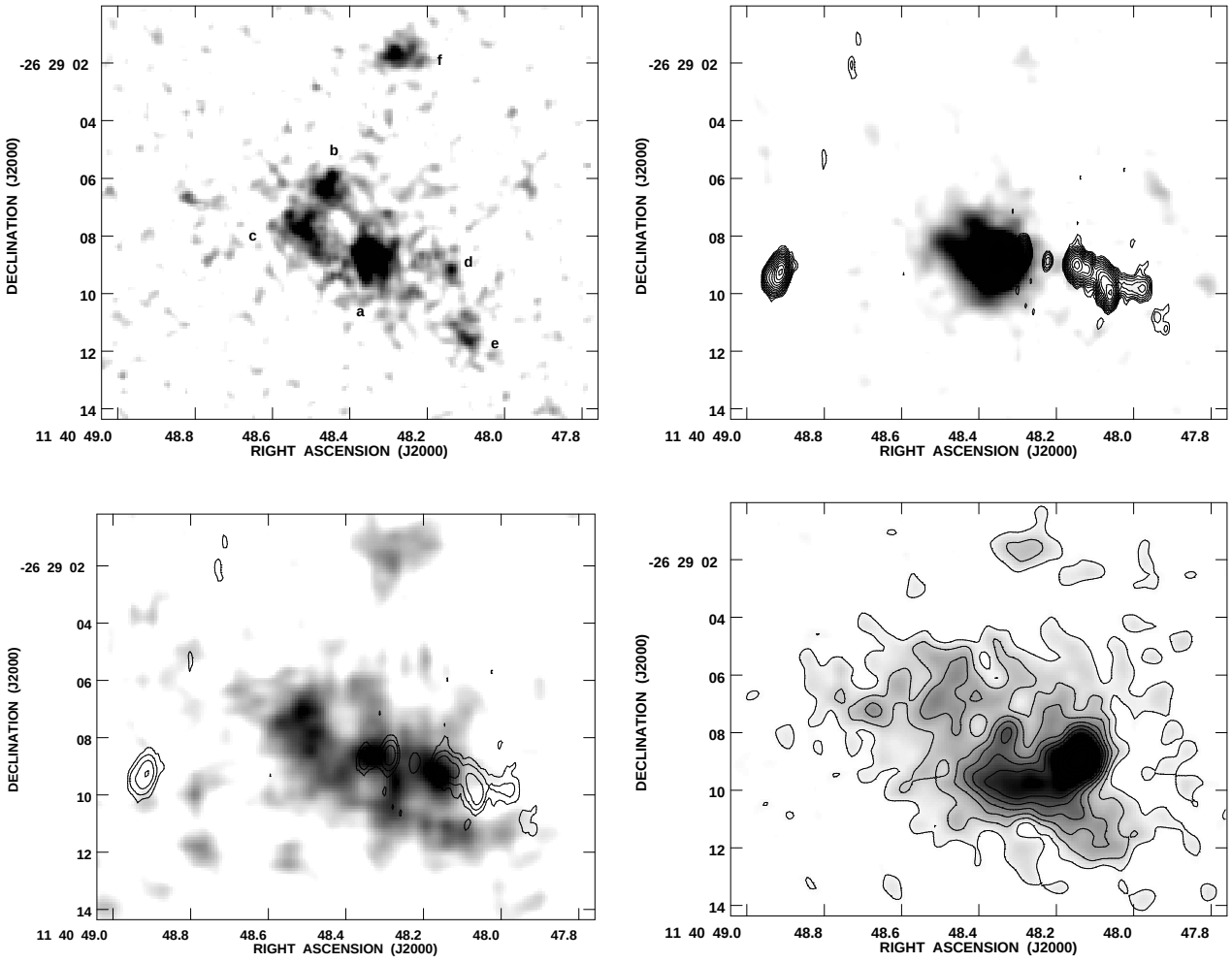

Fig. 4. a r-band image of 1138−262. Labels identify the different components as explained in the text. **b** K_s-band image of 1138−262 with the contours of the 8.1 GHz radio image overlaid. Radio contours are as in Fig. 1b. **c** Smoothed B-band image of 1138−262 with the contours of the 8.1 GHz radio image overlaid. Radio contours are a geometric progression in step of 4 with the first contour level at 0.11 mJy. **d** Image of the extended Lyα emission associated with 1138−262. Contours are linearly spaced at 2σ, 4σ, 6σ etc, where σ is the background rms noice.

Table 4. Physical parameters from the radio emission

Comp.	$P^a_{4.5GHz}$ $\times 10^{34}$ erg s^{-1} Hz^{-1}	L_{TOT} $\times 10^{44}$ erg s^{-1}	B_{min} $\times 10^{-4}$ Gauss	u_{min} $\times 10^{-9}$ erg cm^{-3}	E_{min} $\times 10^{58}$ ergs	P_{min} $\times 10^{-9}$ dyn cm^{-2}
Int.	19.2	43.4				
A	6	14.2	8.5	66	17.9	22
N	0.55	0.92	3.6	12	3.2	4
B1	1.75	2.9	5.0	24	6.3	8
B2	0.16	0.36	3.0	9	2.3	3
B3	4.0	9.0	10	92	24	31
B4	4.8	10.6	6.3	35	9	12
B5	1.2	2.57	4.2	16	4.1	5
B6	0.4	0.82	3.1	8	2.1	3

[a] 4.5 GHz in the rest frame of the radio source.

Baum and Heckman 1989a). For the typical source parameters we find that the external density ranges from $10^{-2}, 10^{-1}$ cm^{-3} for ram pressure confinement, to a few cm^{-3} for confinement by thermal pressure.

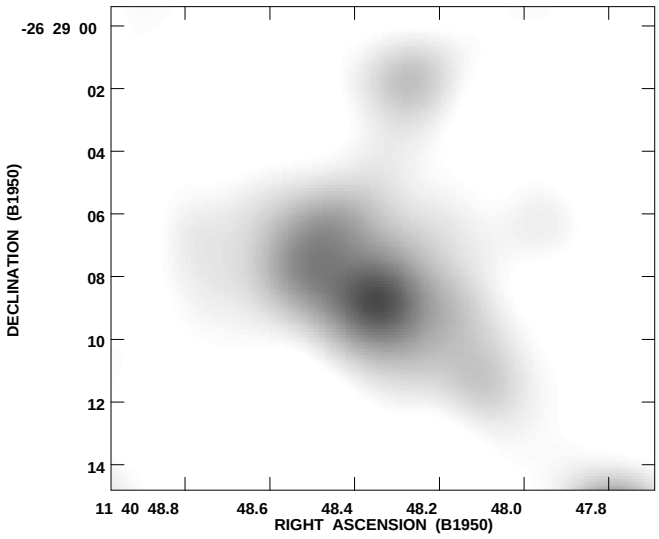

Fig. 5. Image of the r-band emission convolved with a Gaussian function of FWHM 2″

3.2. Optical and IR continuum

In Fig. 4a we present the r-band image. The radio source is identified with an object that is clumpy and roughly oriented along the radio axis. The total optical extension is $\sim 8'' \times 4''$ and the integrated magnitude, measured inside a polygonal aperture which includes all the brightest clumps, is r = 21.7. There are no bright emission lines falling in the wavelength range covered by the r-band filter used, so the image represents the continuum emission from 1138−262. The same r-band image, convolved with a Gaussian of FWHM 2″ to enhance the fainter extended emission, is presented in Fig. 5.

In Fig. 4c we present an image of the B-band emission, smoothed with a Gaussian function having a FWHM of 1″. The B-band is marginally contaminated from line emission: the Lyα emission falls at the lower end of the B-band, where the efficiency of the filter is low. An upper limit for the line contribution is $\sim 10\%$. It is particularly interesting to note that several of the peaks on the B-band image do not coincide with any of the r-band components.

Finally an image of the K_s-band emission overlaid with the 8.1 GHz radio contours is presented in Fig. 4b. In this infrared color the galaxy has a smoother shape: the emission peaks at $11^h40^m48.35^s$, $-26°29'8.9''$, and has an extension of 6″ at a 2σ emission level, in the direction of the radio axis. It is spatially coincident with the supposed nucleus of the radio galaxy and the brightest component in the r-band, with two short "tails" that seem to point in the direction of the components *b* and *c* appearing in the r-band image.

The total magnitude measured through an 8″ diameter aperture is 16.07, but line emission might contribute for a significant fraction. At z = 2.156 the emission lines Hα+[NII]6584,6548 fall in this band. The strength of these lines can be estimated from the Lyα flux, assuming a Lyα/Hα as found for other radio galaxies. This issue will be discussed in Sect. 4.3.

3.2.1. Structure and orientation

We now discuss in detail the following components (as identified in the r-band image): (i) the nucleus, or brightest component; (ii) the smaller clumps that form the main body of the galaxy; (iii) the extended fainter emission and (iv) the small associated object that is detected $\simeq 7''$ to the north of the radio galaxy. A number of features have been labelled for reference in Fig. 4a and Table 6 lists some parameters of the clumps, such as their peak positions, sizes, r-magnitudes measured inside circular apertures of such dimensions and the optical color index B-r relative to component *a*. The brightest component of the galaxy is indicated in Fig. 4a as *a*.

It peaks at $11^h\ 40^m\ 48.35^s$, -26° 29′ 8.8″, and has an r-magnitude of 22.9 within an aperture of 1.1″ radius, which means that its flux is about a third of the total flux of the galaxy. It coincides, within the astrometric uncertainties, with the radio component N identified as the active radio core (the offset is $0.2'' \pm 0.7''$ in declination) and with the the peak of the emission in the K_s-band, which is the reason we believe it is the "nucleus" of the optical galaxy. We distinguish four other smaller components, labelled with letters from *b* to *e*, with r-magnitude ranging from 23.3 to 24.5 and angular sizes of the order 2″ or less, corresponding to linear diameters between 10 and 15 kpc. All clumps have irregular, resolved structures. In Fig. 5 fainter extended emission is revealed, well beyond the clumps: this "halo" has a total extension approximately of $12'' \times 6''$ corresponding to $\simeq 100 \times 50$ kpc^2 in the adopted cosmology and has a curved shape.

A small line emission object is detected $\simeq 7''$ north of the brightest component, both in the r and B-band and only marginally (few σ level) in the K_s-band. It is indicated in Fig. 4a as *f* and has an integrated r-magnitude of 23.9 within a circular aperture of radius 0.8″. This component is also clearly detected (the integrated flux being 60σ where σ is the background RMS

Table 5. Observational parameters of the optical continuum.

Component	RA J2000	Decl J2000	Aperture arcsec	r-mag[a]	B-r[b]
Galaxy	$11^h\ 40^m\ 48.35^s$	-26° 29′8.81″		21.7[c]	
a	48.35^s	8.8″	2.2″	22.9	Ref
b	48.46^s	6.4″	1.6″	23.6	-0.25
c	48.51^s	7.8″	2.0″	23.3	-0.4
d	48.14^s	9.2″	1.6″	24.5	-1.0
e	48.09^s	11.7″	1.6″	24.3	-0.5
f	48.29^s	1.6″	1.6″	23.9	-0.15

[a] Inside a circular aperture of diameter listed in this table.
[b] Optical color index relative to component *a*.
[c] Inside a polygonal aperture including all components except *f*.

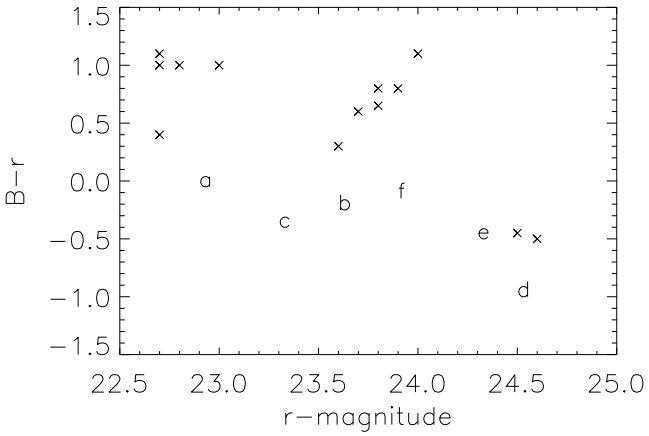

Fig. 6. Plot of the relative color index B-r versus r-magnitude for the components defined in Table 5 (letters) and for extended objects in the near field of 1138−262 (crosses). See text for details.

noise) in the narrow band image: if the line is Lyα, then *f* is at the same at the same redshift as 1138−262, i.e. a companion galaxy of the radio source.

We define the principal axis of the optical galaxy as the line passing through the two brightest peaks (peak position of components *a* and *c*). The angle between the radio axis, defined as the line passing through components A,N and B1, and the optical position is then $29^\circ \pm 2^\circ$. Such alignments between optical and radio morphologies are a common feature of high redshift radio galaxies (e.g. Chambers et al. 1987, McCarthy et al. 1987).

3.2.2. Optical color index

From a comparison of the images of 1138−262 in the different colors bands, it is clear that, as wavelength decreases, there are dramatic changes in the morphology. Since the B-band data are non-photometric, it has been possible to determine only a relative optical color index B-r, For simplicity we choose the central component *a* as reference: we then compute the optical color index of the other components from the counts in the B-band and r-band per unit time, normalized by the same quantities computed for the central component A. It is important to notice that the component have been defined in the r-band, while clearly some of the peaks in the B-band do not coincide with any "labelled" component. Therefore they don't represent necessarily the bluest regions.

A map of the optical color index distribution is also presented in Fig. 7. This has been obtained by smoothing both images with a Gaussian of FWHM 1″, and computing the color index only for those regions where the flux in *both* bands is more than 2σ the RMS background noise. The normalization was done using the number counts of the inner 0.5″ of component *a*. The smallest features, such as the gradients at the edges, are artifacts, due to lower signal to noise. The external regions are systematically bluer than the central region and this trend is particularly evident along the direction of the radio axis. The bluest region is component *d*, which has a B-r index of −1.0, and *e* with a color index of −0.5; also component *c*, which lies along the jet direction, is rather blue (−0.4). In comparison component *f* has almost the same color index as the central part, the difference being only −0.15.

There is a tendency for the fainter components to have bluer color as we can see in Fig. 6, where we have plotted the relative color index versus the r-magnitude. In this figure we have also plotted, as crosses, the relative color index for all the extended objects, which are brighter than 24.5 magnitude in the r-band and are detected at more than a 10σ level in the B-band, in a field of 1.5′ around 1138−262. As we can see the components of the radio galaxy have on average a bluer B-r index than field objects of comparable magnitude.

3.3. The Lyα emission gas

3.3.1. Narrow band imaging

A contour image of the Lyα emission from 1138−262 is shown in Fig. 4d. The radio galaxy 1138−262 exhibits a very common trend seen in powerful radio galaxies (McCarthy 1993a): the emission line gas is distributed asymmetrically with respect to the nucleus and the emission is brightest on the side of the radio lobe closest to the nucleus, suggesting interaction between the radio source and the ambient gaseous medium.

As evident from Fig. 4d, not only the Lyα emission is asymmetric, but it also has a very complex morphology. The gas extends over a region of approximately $13'' \times 7''$. We distinguish several features:
(1) the brightest emitting clump with a maximum at $11^h\ 40^m\ 48.14^s$, -26° 29′ 8.9″ and spatially coincident, within the astrometric uncertainties, with the radio knot B3 (the difference between the peak positions of the radio knot and the gas emission is $0.15'' \pm 0.7''$).
(2) Extended low surface brightness emission, on the scale of $10 - 12''$ with several peaks, none of which coincides with the optical continuum components. It is interesting to notice that the emission extends towards the south east, roughly in the direction of the radio hotspot B4 and its tail, but drops very steeply to the east of the bright emitting component (1).
(3) A relative minimum of Lyα emission, which is positionally coincident with the radio components N and B1. It seems that

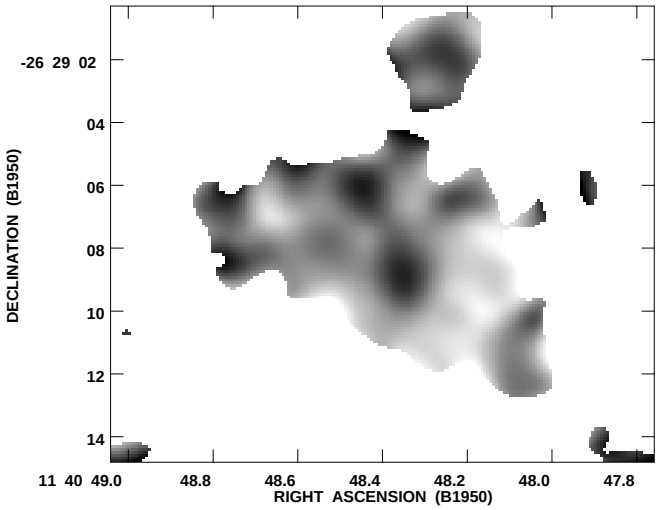

Fig. 7. A grey scale representation of the relative color index distribution of the optical emission from 1138−262. Only regions where the signal is 2σ above the background noise at both wavelengths are considered. The grey scale ranges from -1.1 (white) to 0 (black).

the radio jet "tunnels" through the gas on the side of brightest emission.
(4) Emission coming from component *f*, as identified in the r-band image.

3.3.2. Kinematics of the gas

The spectrum with the slit position almost along the radio axis (PA 77° with respect to the north-south direction) shows the velocity field of the spatially extended Lyα emission. In Fig. 8a we present a one dimensional spectrum of 1138−262, which was extracted by summing over a 14″ region of the slit length: such a large aperture includes all the signal from the fainter, extended emission at a level of 2σ above the background RMS noise. This extension is consistent with the size of the emission along the slit direction that we measure from the narrow band image.

We also present a second spectrum, extracted with an aperture smaller than 4″, centered on the peak of the emission, which includes only the brightest component (Figure 8b). In Fig. 10 we show the two dimensional spectrum, smoothed with a Gaussian function of FWHM 3 pixels (1.1″ in the spatial direction) to enhance fainter extended Lyα emission. Finally in Fig. 9 we present a plot of the spatial profile of Lyα emission (along the slit direction), summed over the full spectral range (60 Å) where the emission was detected at a 2σ level. It clearly shows a bright peak, and a secondary maximum with an offset of 5″.

The structure of the spectrum is very complex and differs in several aspects from that seen in other known high redshift galaxies: here we discuss the kinematics of the components identified in the narrow band image, i.e the brightest emitting clump, the secondary clumps, and the fainter extended emission. Component *f* is not included since it is located outside the slit. The brightest Lyα emission clump peaking at $11^h\ 40^m\ 48.14^s$, -26° 29′ 8.9″ and spatially coincident with the radio component B3, is the compact component in the 2-D slit spectrum. It can be well fitted by a Gaussian profile, centered at 3824 Å and with a relatively low velocity dispersion (FWHM $\sim 650\,\mathrm{km\,s^{-1}}$). As it is evident from a comparison between Figs. 8a and 8b, all the emission comes from a region smaller than 4″. The extended emission, after subtraction of the bright compact component, peaks at 3837Å and has an extension of 14″ along the slit. The overall velocity dispersion is of $\sim 1500\,\mathrm{km\,s^{-1}}$ (FWHM) and there is no evidence of large scale ordered motions, such as rotation. The velocity offset of the compact component with respect to this extended emission, is $1000 \pm 50\,\mathrm{km\,s^{-1}}$ to the blue, suggesting that the cloud is being accelerated towards us, probably from the interaction with the radio jet (see Sect. 4.4.1) In the 2-dimensional spectrum we actually distinguish several peaks, at 3837Å, at 3845 Å and 3853 Å, each with a different spatial offset along the slit, respectively $\simeq 1''$, $\simeq 7''$ and $\simeq 2.5''$ from the brightest, compact feature. Possible interpretation of these peaks and dips include: (i) absorption of the line emission by intervening neutral gas clouds. This kind of absorption has been observed in many HZRGs and quasars (van Ojik 1995). In the case of 1138−262 the absorbers, when modelled with a Voigt profile (van Ojik 1995), would have column densities of the order $logN(HI)_2 \simeq 15-16$ and Doppler parameters between 40 and $100\,\mathrm{km\,s^{-1}}$. However the fit of the various components is not particularly good; (ii) chaotic motions of different gas clouds, resulting from hydrodynamical interaction with the radio plasma. The radio jet accelerates and disturbs the emission line gas as it propagates outwards, destroying any possible sign of ordered motion; (iii) gravitational origin (Heckman et al. 1991). In a dense medium the gravitational potential can be such that gas falling in from large radii can reach velocities of the order $1000\,\mathrm{km\,s^{-1}}$ and more. The presence of different components with net velocity offsets can then be explained with individual gas clouds falling in at successive times.

3.3.3. Ionization, density and confinement of the gas

Different mechanisms have been considered to account for the ionization and the spatial distribution of the extended emission line clouds in powerful radio galaxies (for an extensive review see Baum and Heckmann 1989). It is commonly accepted that the dominant mechanism is photoionization by anisotropically emitted nuclear radiation, which is able to reproduce well both the observed line ratios and the alignment of the ionized gas with the radio axis, observed in many HZRGs (Baum et al. 1990b, Baum et al. 1990a). Other processes, where feasible, can account only partially for the emission or can be important locally (e.g. Robinson et al. 1987).

The natural explanation for the extended, aligned gas emission observed in 1138−262 is photoionization from the nuclear radiation: the line ratios from the low resolution spectroscopy (van Ojik 1995) agree with those predicted by this photoionization mechanism. However additional mechanisms are required to explain the large extension of the emission perpendicular to the radio axis, and in particular the emission from component

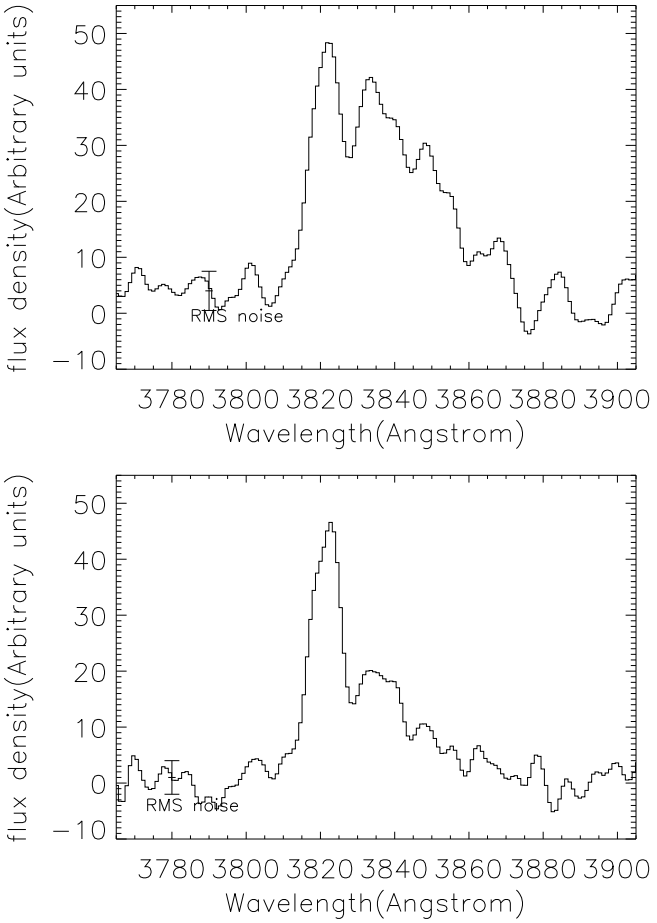

Fig. 8. The spectral profile of the Lyα emission at high resolution, extracted with an aperture of 4″(upper panel) and 14″ (lower panel). Details are described in the text.

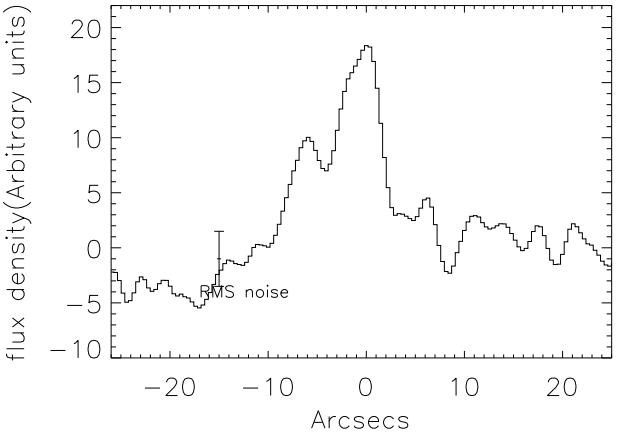

Fig. 9. Spatial profile of the Lyα emission, summed over the full spectral range where Lyα emission was detected.

f since, according to the conventional anisotropic photoionization model, nuclear photons emerge only along the radio axis and do not escape perpendicular to it. Two mechanisms which may well play a role in the ionization of the gas in 1138−262 are ionization by the UV radiation from young, hot stars mixed with the line-emitting gas and shock ionization caused by the interaction between the gas and the radio jet.

From multicolor observations of 1138−262, McCarthy et al. (1997, in preparation) report a total flux at 1500Å of 3.1 μJy. From the flux at 1500Å we can derive the *current* star formation rate (SFR) using the result of Steidel et al. (1996), who find that a specific luminosity at 1500Å of L_{1500} = $10^{40.1}$ ergs s^{-1} Å^{-1} is produced by a SFR of $1 M_{\odot}$yr^{-1}. The derived SFR for 1138-262 is of the order of $90 M_{\odot}$ yr^{-1}. Following the work of Charlot and Fall (1993), who find a Lyα luminosity of $\simeq 8 \times 10^{41}$ ergs s^{-1} for a SFR of $1 M_{\odot}$yr^{-1}, we find that this population of young star could produce all of the observed Lyα emission. For a broad range of models Charlot and Fall also predict that photoionization from massive stars can produce an equivalent width $E_W \simeq$ 100Å, consistent with our data on 1138−262. However note that this mechanism alone cannot explain all the emission, since there is no spatial connection between the optical and the line emission.

Finally the equivalent width of the peak emission (E_W = 260Å) is consistently higher (although not incompatible) than what expected to be produced by hot stars (Charlot and Fall 1993). The positional coincidence of the strong peak of ionized emission and the location where the radio jet bends towards south and the higher equivalent width are strong hints that in this region there is a contribution from shock ionization caused by the interaction between the gas and the radio jet.

In conclusion we favor a model in which the extended emission is due to a combination of photoionization from nuclear radiation and from young hot stars, the emission from component *f* is due to young hot stars and the brightest peak is due to shock ionization.

Given that the photoionization mechanism is not the only one responsible for the line emission, we can still consider it as the dominant mechanism and use it to estimate the density and total mass of the emission line gas from the flux and extent of the Lyα emission line gas, following the approach used by other authors (McCarthy et al. 1990, Chambers et al. 1990). The total inferred mass is $2.5 \times 10^8 M_{\odot}$ and the density $\simeq$ 40cm^{-3}, which are both in the typical range found for HZRG (van Ojik 1995).

We can check the validity of this result by assuming that the emission line clouds are confined by the external pressure exerted by a hot ($\simeq 10^7 K$) medium: confinement of the hotspot require densities of the order 0.1 cm^{-3} (see Sect. 3.1.3). Hence assuming pressure balance between the hot halo gas and the emission line gas at a temperature of $10^4 K$ gives an average density of 100 cm^{-3} of the same order as the density derived above.

Given the uncertainties associated with the two methods our final values for gas densities and masses are necessarily order of magnitude estimates.

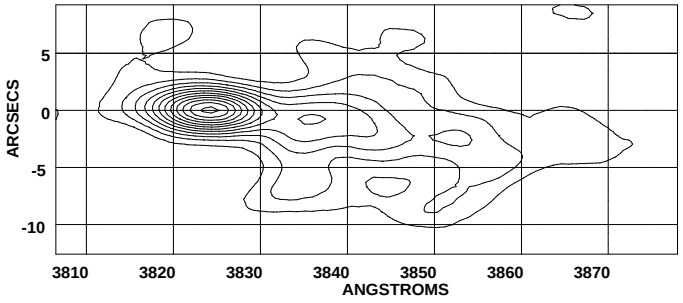

Fig. 10. A two dimensional representation of the high resolution spectrum of Lyα. The origin of the spatial dimension has been arbitrarily set to coincide with the emission peak. The spectrum has been smoothed with a Gaussian of FWHM 1.1″. Contours are linearly spaced at 2σ, 4σ, 6σ, etc where σ is the background rms noise.

Table 6. Observational parameters of the line emitting gas

Comp.	Size kpc	λ_0 Å	FWHM km s^{-1}	Flux 10^{43} erg s^{-1}	E_w^d Å
Total	110[a]		1500	4.5	100
Brightest peak	20[b]	3824	650	2.0[c]	260
2nd brightest peak	40[b]	3837	1000	0.5[c]	120

[a] Total size along the slit.
[b] Size at FWHM along the slit.
[c] Approximate flux.
[d] Rest frame equivalent width.

4. Discussion

4.1. The peculiar properties of 1138−262

The radio galaxy 1138−262 possesses several extreme or unique characteristics which deserve discussion:
(i) The optical continuum (r and B-band) morphology of 1138−262 is amongst the clumpiest of all HZRGs.
(ii) The radio morphology is the most distorted and clumpy of all known powerful HZRGs, consisting of a series of knots and showing a double bend towards south in the eastern lobe.
(iii) The radio nucleus (if detected) has a radio spectral index which is amongst the steepest in all known HZRGs.
(iv) Contrary to virtually all powerful radio galaxies the radio spectral index distribution steepens with distance from the nucleus of the galaxy.
(v) The rotation measure in the western lobe (6200 rad m^{-1}) is the highest measured yet for $z > 2$ radio galaxies and the gradient of RM across the source is also one of the highest.
(vi) The optical color index B-r of the external regions is systematically bluer than the central part.
(vii) While the optical continuum is very clumpy, near infrared imaging shows an extremely bright (K-band magnitude is 16.07) and compact object.
(viii) There is a small companion object in a direction perpendicular to the radio axis, which is gas rich.
(ix) The distribution of the Lyα emission gas does not follow the optical continuum. The peak of the line emission does not coincide spatially with the central part of the optical galaxy, but with the location at which the radio jet bends.
(x) The inner part of the radio jet seems to tunnel through the gas.

4.2. Companion galaxy

There are two reasons to believe that the object labelled *f* in Fig. 4a is at the same distance as the radio galaxy: first, this component appears in the Lyα narrow band image with an approximate flux of 10^{42} erg sec^{-1}. From the continuum emission level in the B-band, if the object didn't have line emission at a wavelength corresponding to the narrow band filter, we wouldn't have detected it in the narrow band. Furthermore the equivalent width of the line (E_w = 85Å), is very close to the equivalent width of the Lyα emission line from 1138-2 62 (E_w = 100Å). Therefore the emission line from component *f* is probably also Lyα, implying that this object is at a redshift of 2.156. A second argument, although less stringent, is that the optical color index B-r of component *f* is similar to that of the host galaxy of 1138-262, while typical field objects of comparable magnitude tend to have a redder color, as shown in Fig. 6.

Extensive studies on companions of radio galaxies have been carried out at low redshift, and in many cases the presence of companion objects has been interpreted as a direct effect of the radio source. The best known case is Minkowsky's object: the location of this dwarf galaxy is at the end of the radio jet emanating from the radio galaxy PKS 0123−016 at z = 0.0181, suggesting that its origin is due to jet-induced star formation (van Breugel et al. 1985). A similar star forming region associated with the nearby powerful radio galaxy 3C285 has also been reported (van Breugel and Dey 1993). Finally, in a sample of USS sources, Rottgering *et al.* (1996c) find evidence that companions of radio galaxies tend to be located along the radio axis : this has been interpreted as an enhancement of the luminosity of dwarf galaxies along this direction due to jet induced star formation.

On the other hand Le Fevre et al., have recently detected two companion galaxies, in the field of the radio galaxy 0316-257 at z = 3.14 and interpreted their observations as a sign that the comoving density of galaxy around high redshift radio galaxies might be significantly higher than the average background density (Févre et al. 1996). The case of 1138−262 fits well in this scenario, since the companion galaxy is not observed along the radio axis direction but in a direction which is perpendicular to it: object *f* lies totally outside the cone in which radiation escapes from the active nucleus, implying that its origin is *not* related directly to the action of the radio source. Its existence can be interpreted as an indication that the environment of the radio galaxy 1138-262 has cluster (or protocluster) like properties. The origin of the ionization of the gas is not clear, but the Lyα equivalent width is consistent with what predicted by models of photoionization by young hot stars(see Sect. 3.4.3). Star formation could have been triggered by the tidal interactions between the dwarf and the main galaxy.

4.3. The nature of the infrared emission

It has been claimed that the continuity in the K−z diagram between low and intermediate redshift galaxies and high redshift radio galaxies is an indication that the much of the K-band light at high z is also stellar (e.g. Lilly 1989, Dunlop et al. 1989, McCarthy 1993b).

The magnitude of 1138−262 in this infrared color is the brightest of all known radio galaxies at redshift $z \sim 2$, and comparable to that of $z \sim 1$ galaxies (McCarthy 1996). Although at $z \geq 2$ the scatter in the K–z diagram increases (McCarthy 1996), the position in this diagram of 1138−262 is striking, being ∼0.8 magnitudes brighter than the second known brightest object at similar redshift and 2 magnitudes brighter than the mean K of $z \sim 2$ radio galaxies. This extremely bright magnitude could be an evidence that 1138−262 is much more massive than other galaxies at similar redshift. Alternatively it could be due to an anomalously large non stellar contribution due to e.g. (i) contamination from the emission lines Hα+[NII]6584,6548; and (ii) contribution by the light emitted by an optically-obscured quasar.

We can estimate the contribution from the emission lines Hα+[NII]6584,6548 from the Lyα emission, assuming a Lyα/Hα ratio. The range of Lyα/Hα quoted in literature is large: while McCarthy et al. (1992) derive modest line contributions ($\sim$ 10%), Eales & Rawlings report substantial Hα contributions for few radio galaxies, on the basis of near-IR slit spectra (Eales and Rawlings 1993). To estimate an upper limit to the line contamination, we will follow Eales & Rawlings who find Lyα/Hα $\sim$ 1 and assume that half the emission from the complex Hα+[NII]6584,6548 actually comes from Hα (Eales and Rawlings 1993). The resulting total contribution of line emission in the K-band is then $\sim$ 25%, implying an increase in magnitude of 0.3 units.

To investigate a possible contribution of a nuclear point source we fit the K-band image with a classical de Vaucouleurs profile plus a point source, following the method outlined in Best et al (1997).

The best–fit model is shown in Fig. 11 and consists of a de Vaucouleurs distribution, having a characteristic radius of $1'' \pm 0.1''$ plus a point source which contributes 6% of the total flux. If we fix the characteristic radius of the de Vaucouleurs distribution, during the fitting procedure the contribution of the central point source is estimated independently and depends upon the fixed effective radius: increasing the radius has the effect of requiring a stronger contribution from the point source as evident from Fig. 12. From this plot we can derive an upper limit for the point source contribution of 18% (∼0.2 magnitudes).

We conclude that at most half of the infrared light comes from non stellar-components. Subtracting this contribution brings the K-band magnitude to 16.8. This result must be interpreted with some caution since the morphology of the gas is unknown: the gas contribution could be much more important in the outer regions, implying that the de Vaucouleurs profile is approximated by the gas emission rather than stellar light. Moreover we have assumed a de Vaucouleurs model, and then estimated the point source needed to match the observed distribution: if the emission does not follow a de Vaucouleurs profile, the point source contribution could be different. A direct determination of both the luminosity and the morphology of the Hα emitting gas would help settle the issue. Taking the above arguments into account, for the remainder of this discussion we shall assume that at least half of the infrared light comes from an old stellar population. From fit of the spectral energy distribution with a 2.5 Gyrs old population of stars plus a starburst involving 0.1% of the mass (McCarthy et al. in preparation), the inferred mass is then $10^{12} M_{\odot}$.

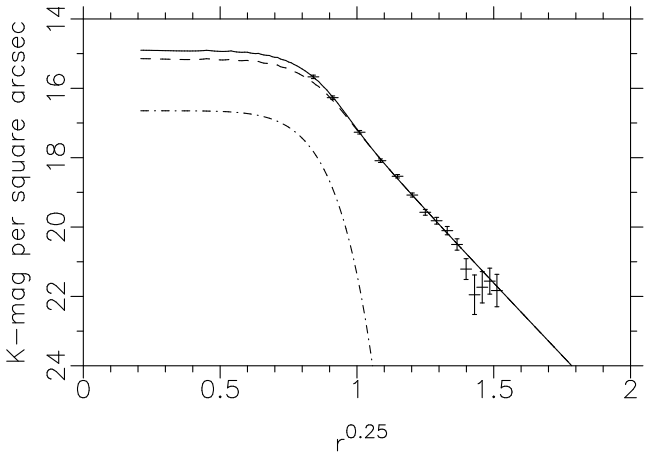

Fig. 11. Data points show the distribution of the K-band emission. The dashed line is the best fit de Vaucouleurs model with a characteristic radius of $1''$, the dash-dotted line is the 6% flux contribution of the point source required to fit the data. The solid line is the sum of the two components.

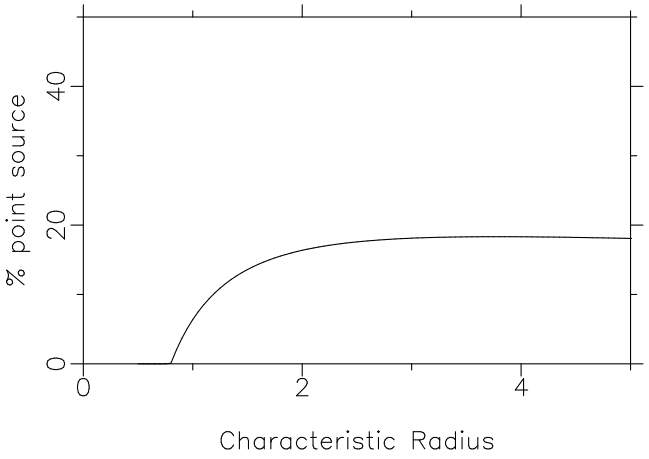

Fig. 12. Percentual flux contribution from a point source required to fit the observed distribution, as a function of a given characteristic radius (see text for details).

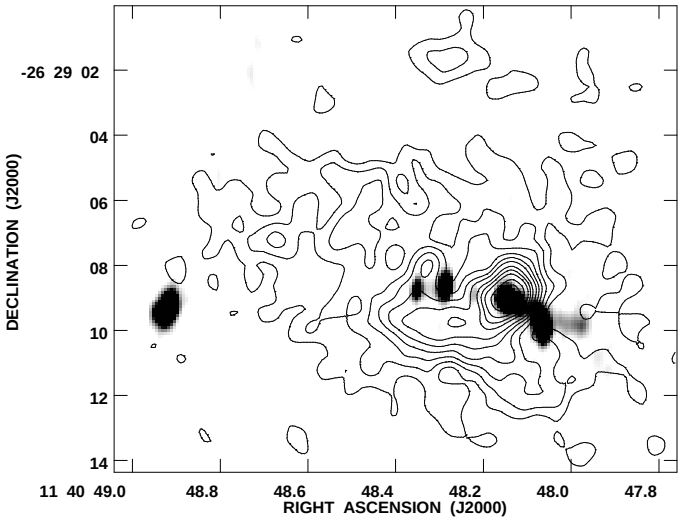

Fig. 13. The Lyα image of 1138−262 in a contour representation, with the 8.1 GHz VLA map in grey-scale superimposed. Radio component B3, the bending point of the western jet, coincides with the peak of the Lyα emission.

4.4. The Lyα-radio source connection

4.4.1. Deflection of the radio jet

The general radio structure of 1138−262, with its multiple knots and extremely distorted morphology, is very different from that of typical powerful radio sources, both at high and low redshift. It resembles that found for some compact steep spectrum (CSS) radio sources (Fanti et al. 1990). In those cases it has been suggested that the complex morphologies may indicate that the propagation of the radio jet is highly constrained by a very dense, clumpy external medium, but while CSS have typical scales of a few kpc, in the case of 1138−262, the bent structure has a scale of more than 50 kpc.

Several authors have discussed multiple hotspots and bending of the radio jets in quasars and radio galaxies (Lonsdale and Barthel 1986, Cox et al. 1991): two general models are favored, one involving changes in the orientation of the beam from the parent object (Scheuer 1982), and the other in which secondary hotspots are formed by collimated outflow of plasma from the primary hotspots (Lonsdale and Barthel 1986).

A remarkable characteristic of 1138−262 is the spatial coincidence of the sharpest bend in the radio jet (hotspot B3) with the peak of the Lyα emission (see Fig. 13): for this reason we find that the most promising model is that by Lonsdale and Barthel (1986), who argue that the double hotspots often seen in radio sources are due to deflection of the radio jet by a gas cloud. They suggest that a possible mechanism for the bend is through a "De Laval" nozzle (Blandford and Rees 1974): the jet burrows into a gas cloud, where it inflates a bubble of ultra hot plasma; the bubble then breaks out at the weakest boundary of the confining cloud creating a De Laval nozzle. A collimated outflow is produced in this new direction and the secondary hotspots are formed by further interaction with the gas. Since the bubble is likely to be highly asymmetric, only one-sided outflows are seen. If the cloud is dense and massive enough, it could preserve the angle of deflection for a time sufficient to build secondary hotspots.

We will show that this mechanism could explain the bent structure of 1138−262, at least at the location of hotspot B3. In particular we will show that the density of the hot halo derived in Sect. 3.1 is sufficient to provide pressure gradients that confine the hotspots, so that there is enough time for the secondary hotspots to be built; that the mass necessary to deflect the jet is consistent with the mass of the ionized gas in the bright emitting clump and that the jet has enough kinetic energy to accelerate the deflecting gas cloud to the measured velocity.

The average energy supply rate to hotspot B5 can be estimated from its total luminosity, assuming a conversion factor of 0.1 (Bridle and Perley 1984), as 2×10^{45} erg s^{-1}. From this and the total minimum energy of component B5 (see Table 4), the time required to build up component B5 is 10^6 years, ignoring energy losses. This value implies that the advance speed of B3 must be $\leq 0.05c$ so that B3 does not pass the other hot spots within the time in which they are built up. From minimum energy density of component B3 and the ram pressure balance equation, $v_h^2 = u_m/(3n_{cl}m_p)$, the density of the deflecting cloud must then be > 0.01 cm^{-3}. Therefore the hot halo, whose presence was suggested in Sect. 3, has a sufficient density to provide the necessary time to build up the secondary hotspot. Of course it is the presence of density gradients that can deflect the radio jet: it is straightforward to assume that the region responsible for the deflection of the jet is the bright emitting clump observed in the narrow band image. This same deflecting "cloud" should then be accelerated by the interaction with the radio-jet, and indeed it appears to have a net velocity of 1000 km s^{-1} with respect to the extended Lyα emission. Assuming that this emitting clump is spherical, the minimal density derived above gives an overall gas mass of few times $8 \times 10^7 M_\odot$. In the previous section we have derived an overall mass of the ionized gas of $2.5 \times 10^8 M_\odot$ of which a fraction is due to the emission from the brightest clump. Therefore these two numbers are in consistent.

The total kinetic energy of the gas cloud with the inferred mass and the observed net velocity of 1000 km s^{-1} is $\simeq 10^{57}$ ergs. The jet power was estimated before as $L_{jet} = 2 \times 10^{45}$ ergs s^{-1}, therefore the time needed to provide the cloud with its kinetic energy is few times 10^4 yr, depending on the transfer efficiency of jet power into kinetic energy, so within the time in which the secondary hotspots are built.

In this deflection scenario, the initial cloud that is hit by the radio jet, could also consist of a region of small dense clouds with lower density gas in between. The interaction with the radio jet may rip apart these dense clouds forming a gaseous medium with an increasing filling factor and covering factor (Bremer et al. 1996): in this medium the De Laval nozzle forms. The larger filling factor would cause a larger fraction of the gas to be exposed to the ionizing radiation and this could partially explain the strong Lyα emission in this region. Finally, shock ionization due to the impact of the jet could also contribute to the gas emission.

4.4.2. Correlation between radio parameters and Lyα emission

We have argued that the spatial coincidence of the radio bend and the peak of the Lyα emission, as well as the high velocity dispersion of the gas are direct evidence that there is a strong interaction between the radio jet and the emission gas. More indirect indications for a strong connection comes from comes from a number of correlations that have been observed between the Lyα emission and the radio parameters for a sample of 18 HZRGs (van Ojik et al. 1997). In particular strong correlations were found between (i) the amount of radio distortion and the gas emission distortion; (ii) the radio size and the Lyα emission size and (iii) the radio size and the velocity width of the Lyα emission.

The properties of 1138−262, although extreme, are consistent with the picture of a strong interaction between the radio source and the Lyα emitting gas.

From the two-dimensional spectrum it is clear that the spatial position of the peak in the Lyα emission varies with wavelength. Following the method used by van Ojik et al.(1996b), we measured the peak position of the Lyα per wavelength bin, with a bin-size of 3 pixels to obtain a good accuracy in the position determination. The peaks were measured in the smoothed frame of Fig. 10. The errors in the peak position depend on the S/N of the emission in each wavelength bin. The results are shown in Fig. 14.

Following van Ojik et al. 1996b we used two parameters to represent the distortion of the spectra: the first is simply the distance between the most extreme Lyα positions, ΔS; the second is the so called "wiggling index" w_s which is equal to the number of different positional gradients of the peak of the Lyα emission and indicates whether there is a smooth gradient in the spectrum, or if there are several bends. For 1138−262 $\Delta S = 4''$ and $w_s = 4$, bot h indicating that the spectrum is one of the most distorted, if compared to the sample of HZRGs studied by van Ojik et al. (1996b). This result together with the fact that 1138−262 has one of the most distorted radio morphologies of galaxies beyond $z = 2$ reinforces the conclusion that the most distorted radio morphologies also has the most disturbed Lyα gas.

The radio size of 1138−262 is large, 127 kpc, which means that it would be the third larger galaxy of the mentioned sample; on the other hand the size of the Lyα halo along the radio axis (at a level of 20% the peak emission) is also very large, $\simeq$ 70 kpc, i.e. the fourth in this sample. So this is consistent with the conclusion that the size of the Lyα emitting gas strongly depend on the size of the associated radio source.

In conclusion our favored interpretation of the data is that the radio source and the emitting gas along the radio jets are strongly coupled. The radio jet stirs the gas along its course, inducing the chaotic motions and the great distortions in the spectrum, as well as enhancing the gas emission by shock ionization at the location of hotspot B3. The interaction is probably the origin of the bent morphology of the jet and the presence of multiple hotspots.

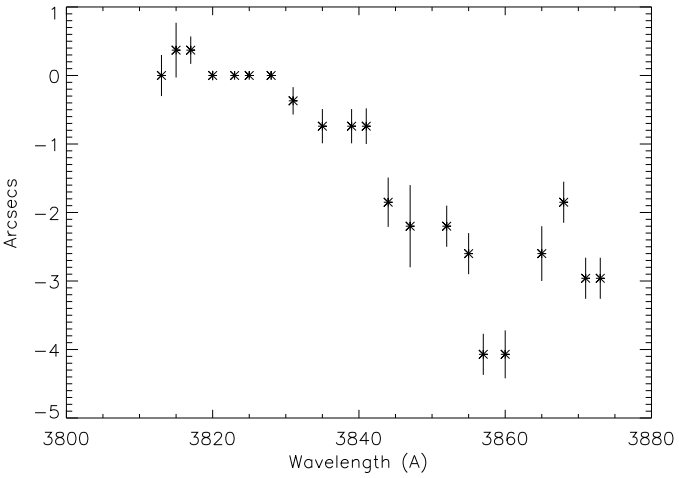

Fig. 14. Position of the the peak of the Lyα emission against wavelength.

4.5. High rotation measure: further evidence that 1138−262 is at the center of a protocluster

In Table 3 we have presented values of depolarization and rotation measure (RM) for the radio components A and B4 (from Carilli et al. 1997).

An essential question is whether the observed RM are galactic in origin or local to the source itself: the interstellar medium in the Galaxy can cause large values of RM only at low galactic latitude, $|b| < 10°$ (Leahy 1987), while 1138-262 is at $b = 34°$; moreover significant gradients in RM on scales $\simeq 10''$ such as that observed in 1138−262, would not be modelled easily via a Galactic screen. Therefore Carilli et al. conclude that the Faraday screen is located at the same redshift as the source. This implies an additional factor of $(1 + z)^2$, bringing the RM to a value of 6200 rad m^{-2} for hotspots A, the highest value measured in all known HZRGs, comparable to the most extreme cases at lower z, and in particular to those observed for the prototypical powerful radio source Cygnus A (Carilli et al. 1991, Perley and Carilli 1996).

A recent result from the study of powerful radio galaxies at the centers of X-ray clusters is a relationship between the cluster X-ray gas density and the magnitude of Faraday rotation observed towards the radio source, independent of source morphology (Taylor et al. 1994). The physical conclusion is that the Faraday rotation is mostly due to the cluster gas which is substantially magnetized, rather than the result of interaction of the source with its environment. Drawing the analogy between low redshift radio galaxies and 1138−262, we can conclude that this galaxy is also likely to be situated at the center of a dense, X-ray cluster gas, possibly with a cooling flow. A mass flow rate as large as $400 - 500 M_{\odot}\mathrm{yr}^{-1}$ would be consistent with the relation found by Taylor et al for low redshift radio galaxies.

However we still have to explain the big gradient in RM between the two hotspot (a factor of 10) and their different depolarization. Depolarization asymmetries have been extensively studied for radio galaxies and quasars (Garrington et al. 1991,

Garrington and Conway 1991). The counter-jet is on average, more depolarized than the jet because it is the most distant, and the observed radiation must pass through a greater fraction of the hot X-ray halos which surround the radio sources (the so called Laing-Garrington effect). In 1138−262 hotspot B4 shows significantly greater depolarization, so in this view it should be the furthest from us. But if this was the case then it should also have a RM equal to or larger than the other hotspot. So there are two apparently contradictory measures.

We notice that the most depolarized jet is on the same side as the emission line gas: we have already presented clear evidence for a strong interaction between the gas and the radio jet. Garrington et al. (1991b) found only little evidence that depolarization is in spatial association with asymmetric extended narrow-line regions. However because they analyze a sample made of radio galaxies and quasars, the effect of the asymmetric distribution could be masked by a possible strong projection effects in quasars. Taking the sample of Garrington et al. (1991b), among the radio galaxies which show a clear asymmetry in the morphology of the emission gas 11 have stronger depolarization on the same side as the emitting gas and only 4 show the opposite, making the result much more significant.

We conclude that the Lyα emission gas is responsible for the strong depolarization of hotspot B: the magnetic field within the gas clouds is tangled only on small scales, therefore there are field reversals and the polarized light emerges from the gas with only little net rotation of the polarization angle. However the polarization plane of light passing through paths which are only slightly different, will be rotated by a different angle, hence the distribution of angles will be spread out, implyi ng depolarization of the measured beam.

Finally the large scale gradients in the RM distribution such as that observed in 1138−262 are a common feature for large RM radio galaxies, and most likely reflect the typical size scale for variations in the magnetic field direction.

4.6. Scenarios of galaxy formation: is 1138−262 a proto-cD galaxy?

One of the principal aims of studying distant radio galaxies is to investigate the process of galaxy formation and to place some observational constraints on the models of formation and evolution of structures in the early universe. Several mechanisms have been invoked in scenarios of galaxy formation:
(i) Inhomogeneous collapse of matter. In a broad class of models galaxies are formed through a generic inhomogeneous collapse of matter: at the location of overdensities in the primordial fluctuation, large gas reservoirs build up and then undergo massive starbursts. White (1989), reviews theoretical expectations for the appearance of galaxies during their formation phase, and concludes that a common idea in most formation theories is that the final assembly of a galaxy is a highly inhomogeneous process, and in particular this must be true for the formation of the stellar population. Hence such models predict that the appearance of a galaxy at the early stage of its formation should be highly irregular and clumpy (Baron and White 1987).
(ii) Hierarchical growth. A second general mechanism postulates that all structures grow hierarchically, small objects are the first to form and then amalgamate into progressively larger systems (White and Rees 1978). Hierarchical scenarios are by far the most frequently investigated models by means of both numerical and analytical work (e.g. Katz et al. 1992, Kauffmann and White 1993, Navarro et al. 1995). In these scenarios giant elliptical galaxies would be formed by merging of several dwarf galaxies. Mergers are believed to be very important also for fueling the central engine of AGNs (Osterbrock 1993).
(iii) Massive cooling flows. In cooling flows mechanisms galaxies form by means of homogeneous collapse of matter at the center of massive cooling flows. It has been argued that massive cooling flows exist at high redshift, and they play an essential role in the formation of giant elliptical galaxies at the center of clusters of galaxies (Bremer et al. 1996, Fabian and Nulsen 1995). The alignment between the major axis of cD galaxies and that of their parent cluster hints that the formation of these two entities are tightly linked (Crawford and Fabian 1995).

Most models, while considering several of the above physical processes as important, emphasize one particular mechanism. Our observational study of 1138−262 indeed suggests that in the actual formation and evolution of galaxies a combination of all these processes occurs. In the previous sections we have presented several independent pieces of evidence that the radio galaxy 1138−262 is situated at the center of a very dense, cluster-type of environment, with the probable presence of a massive cooling flow. Furthermore in Sect. 4.3 we have shown that the host galaxy of 1138-262 is a well formed elliptical galaxy, with a morphology which is well fit by a de Vaucouleurs distribution, and an old stellar population which is the most massive of all known radio galaxies at similar redshift. These observations therefore support the idea that giant elliptical galaxies would form at the center of massive cooling flow clusters. In the context of our observations of 1138-262, a cooling flow would also be a possible mechanism to explain the presence of the large amount of gas observed on a large scale.

Our observations of 1138-262 lend support also to the hierarchical or inhomogeneous models for structure formation. The deep NTT images in the optical/near UV show in fact a very inhomogeneous morphology, consisting of a central region, coinciding with the infrared galaxy, and of a number of clumps well further this core. This external components have an optical index which is systematically bluer than that of the nucleus, suggesting that they contain a much younger stellar population and have the typical size scales of dwarf galaxies. Determining the spectral energy distribution of these single clumps would establish whether they are simply star forming regions that will be accreted by the parent galaxy, or well formed dwarf galaxies, companions of the 1138-262 host in the surrounding cluster, that might eventually merge with it.

We conclude that the host galaxy of 1138-262 is likely to be a massive elliptical galaxy, formed at the center of a dense, cluster like medium, possibly with a cooling flow, which is ac-

creting even more mass from its very dense environment and will therefore become even more massive. We therefore suggest that 1138−262 is a proto-cD galaxy at the center of a cluster.

5. Conclusions

We have presented an observational study of 1138−262, a radio galaxy at a redshift of z = 2.156. This object has extreme properties in the radio, in the optical continuum and in the line emission. We have argued that the observations have the following implications:
(i) The radio source resides at the center of hot (T=10^7 K), Xray emitting cluster atmosphere with high core density. Support comes from the extreme rotation measure, arguments regarding the confinement of the emission line gas and radio hotspots and the presence of a small companion galaxy, whose origin is not due to the presence the radio source.
(ii) The host galaxy of 1138−262 could be the progenitor of a present day cD galaxy. From the K-band magnitude we derive a mass of the order $10^{12} M_{\odot}$ and there are evidences that it is accreting more mass from its very dense environment, where star formation is currently taking place, therefore becoming even more massive.
(iii)The spatial coincidence of the sharpest bent of the western radio jet and the peak of the emission line gas suggests that a massive gas cloud is responsible for the bend. We have shown that a mechanism that is consistent with the physical parameters could be bending through a de Laval nozzle.
(iv)The radio jets are strongly interacting with the surrounding gas and have a profound influence of the morphology and kinematics of the Lyα emission gas. The observed chaotic motions and the high velocity dispersion of the gas are probably due to this interaction.
(v) The bluer optical color index of the regions along the radio axis direction, support the idea that star formation is those regions is induced by the passage of the radio jet.

Two upcoming important observations will help us check some of our conclusions: first ROSAT measurements could confirm the existence of the X-ray cluster gas around this high redshift galaxy. Then high resolution HST images of 1138−262 will allow us to investigate further this unique radio galaxy. Preliminary results from the HST survey of distant radio galaxies show that clumpiness is a very common characteristic of these objects. A more systematic study of this phenomenon will allow us to put some constraint on models for galaxy formation and evolution.

Acknowledgements. We would like to thank Simon White for reading to manuscript and giving very helpful comments. We also thank Philip Best for his kind help and useful discussions. HJAR acknowledges support from an EU twinning project, a programme subsidy granted by the Netherlands Organisation for Scientific Research (NWO) and a NATO research grant.

References

Baron, E. and White, S. D. M.: 1987, ApJ **322**, 585
Baum, S. A., Heckman, T., and van Breugel, W.: 1990a, ApJS **74**, 389
Baum, S. A. and Heckman, T. M.: 1989a, ApJ **336**, 681
Baum, S. A. and Heckman, T. M.: 1989b, ApJ **336**, 702
Baum, S. A., O'Dea, C. P., Murphy, D. W., and de Bruyn, A. G.: 1990b, A&A **232**, 19
Best, P., Longair, M. S., and Röttgering, H. J. A.: 1997, MN: in preparation
Blandford, R. D. and Rees, M. J.: 1974, MNRAS **169**, 395
Bolton, J. G., Wright, A. E., and Savage, A.: 1979, Aust. J. Phys. Astroph. Suppl. **46**, 1
Bremer, M. N., Fabian, A. C., and Crawford, C. S.: 1996, MNRAS, submitted
Bridle, A. H. and Perley, R. A.: 1984, ARA&A **22**, 319
Carilli, C. L., Perley, R., Dreher, J. W., and Leahy, J. P.: 1991, ApJ **383**, 554
Carilli, C. L., Röttgering, H., van Ojik, R., Miley, G. K., and van Breugel, W.: 1997, APJ: in press
Chambers, K. C., Miley, G. K., and van Breugel, W.: 1987, Nat **329**, 604
Chambers, K. C., Miley, G. K., and van Breugel, W. J. M.: 1990, ApJ **363**, 21
Charlot, S. and Fall, S. M.: 1993, ApJ **415**, 580
Cox, C., Gull, S., and Scheuer, P.: 1991, MNRAS **252**, 558
Crawford, C. and Fabian, A.: 1989, MNRAS **239**, 219
Crawford, C. S. and Fabian, A. C.: 1995, MNRAS **273**, 827
Dunlop, J., Guilderoni, B., Rocca-Volmerange, B., Peacock, J., and Longair, M.: 1989, MNRAS **240**, 257
Dunlop, J. S. and Peacock, J.: 1993, MNRAS **263**, 936
Eales, S. and Rawlings, S.: 1993, ApJ **411**, 67
Elias, H., Frogel, J., Matthews, K., and G.Neugebauer: 1982, AJ **87**, 1029
Fabian, A. and Nulsen, P.: 1995, MNRAS **277**, 561
Fanti, R., Fanti, C., Schilizzi, R. T., Rendong, N., Parma, P., van Breugel, W. J. M., and Venturi, T.: 1990, A&A **231**, 333
Févre, O. L., Deltorn, J., Crampton, D., and Dickinson, M.: 1996, ApJ **471**, L11
Garrington, S. and Conway, R.: 1991, MNRAS **250**, 198
Garrington, S., Conway, R., and Leahy, J. P.: 1991, MNRAS **250**, 171
Heckman, T. M., Lehnert, M. D., van Breugel, W., and Miley, G. K.: 1991, ApJ **370**, 78
Katz, N., Hernquist, L., and Weinberg, D. H.: 1992, ApJ **109**, 399L
Kauffmann, G. and White, S.: 1993, MNRAS **261**, 921
Laing, R. A.: 1988, Nature **331**, 149
Landolt, A. U.: 1992, AJ **1**, 104
Lasker, B., Sturch, C. R., McLean, B. J., Russel, J. L., Jenker, H., and Shara, M.: 1990, AJ **99**, 2019
Leahy, J. P.: 1987, MNRAS **226**, 433
Lilly, S. J.: 1989, ApJ **340**, 77
Lonsdale, C. J. and Barthel, P.: 1986, AJ **92**, 12
Lonsdale, C. J., Barthel, P., and Miley, G.: 1993, ApJS **87**, 63
McCarthy, P.: 1996, in M. Bremer, C. Carilli, H. Röttgering, and P. van der werf (eds.), Cold Gas at High Redshifts, Kluwer
McCarthy, P., Kapahi, V., Breugel, W. V., Persson, S., Athreya, R., and Subrahmanya, C.: 1996, ApJS **107**, 19+
McCarthy, P., Spinrad, H., van Breugel, W., Liebert, J., Dickinson, J., Djorgovski, S., and Eisenhardt, P.: 1990, ApJ **365**, 487
McCarthy, P., van Breugel, W., Spinrad, H., and Djorgovski, S.: 1987, ApJ **321**, L29
McCarthy, P. J.: 1993a, ARA&A **31**, 639
McCarthy, P. J.: 1993b, PASP **105**, 1051
McCarthy, P. J., Persson, S. E., and West, S. C.: 1992, ApJ **386**, 52

Miley, G. K.: 1980, ARA&A **18**, 165
Muxlow, T. W. B. and Garrington, S. T.: 1991, in P. A. Hughes (ed.), Beams and Jets in Astrophysics, p. 232, Cambridge University Press Cambridge
Navarro, J., Frenk, C., and White, S.: 1995, MNRAS **275**, 56
Osterbrock, D. E.: 1993, ApJ **404**, 551
Pascarelle, S. M.,Windhorst, R. A.,Keel, W. C., and Odewahn, S. C.: 1996, nat **383**, 45
Perley, R. A. and Carilli, C.: 1996, in C. Carilli and D. E. Harris (eds.), Cygnus A: Study of a Radio Galaxy, p. 168, Cambridge University Press
Persson, S., West, S., Carr, D., Sivaramakrishnan, A., and D.C.Murphy: 1992, PASP **104**, 204
Robinson, A., Binette, L., Fosbury, R., and Tadhunter, C. N.: 1987, MNRAS **227**, 97
Röttgering, H., Hunstead, R., Miley, G. K., van Ojik, R., and Wieringa, M. H.: 1995, MNRAS **277**, 389
Röttgering, H. and Miley, G. K.: 1996, in J. R. Walsh and I. Danziger (eds.), Science with the VLT
Röttgering, H. J. A., Lacy, M., Miley, G., Chambers, K., and Saunders, R.: 1994, A&AS **108**, 79
Röttgering, H. J. A., West, M., Miley, G., and Chambers, K.: 1996, A&AS **307**, 376
Scheuer, P. A. G.: 1982, in D. Heeschen and C. Wade (eds.), Extragalactic Radio Sources, p. 345, IAU Symposium no. 97, Dordrecht: Reidel
Steidel, C. C., Giavalisco, M., Pettini, M., Dickinson, M., and Aldebergerw, K. L.: 1996, ApJ **462**, 17
Taylor, G., Barton, E., and Ge, G.: 1994, AJ **107**, 1942
van Breugel, W. and Dey, A.: 1993, ApJ **414**, 563
van Breugel, W., Filippenko, A. V., Heckman, T. M., and Miley, G.: 1985, ApJ **293**, 83
van Ojik, R.: 1995, Ph.D. thesis, University of Leiden
van Ojik, R., Röttgering, H., Carilli, C., Miley, G., and Bremer, M.: 1996a, A&A **313**, 25
van Ojik, R., Röttgering, H., Miley, G., Bremer, M., Macchetto, F., and Chambers, K.: 1994, A&A **289**, 54
van Ojik, R., Röttgering, H. J. A., Miley, G. K., and Hunstead, R.: 1996b, A&A: A&A **317**, 538
White, S. D. M.: 1989, in C. Frenk, R. Ellis, T. Shanks, A. Heavens, and J. Peacock (eds.), The Epoch of Galaxy Formation, p. 10, Dordrecht: Kluwer
White, S. D. M. and Rees: 1978, MNRAS **341**, 183

This article was processed by the author using Springer-Verlag TEX A&A macro package version 3.